



# Intrinsically Disordered Bacterial Polar Organizing Protein Z, PopZ, Interacts with Protein Binding Partners Through an N-terminal Molecular Recognition Feature

Christopher T. Nordyke <sup>1</sup>, Yasin M. Ahmed <sup>2</sup>, Ryan Z. Puterbaugh <sup>1</sup>, Grant R. Bowman <sup>2\*</sup> and Krisztina Varga <sup>1\*</sup>

- 1 Department of Molecular, Cellular and Biomedical Sciences, University of New Hampshire, Durham, NH 03824, United States
- 2 Department of Molecular Biology, University of Wyoming, Laramie, WY 82071, United States

Correspondence to Grant R. Bowman and Krisztina Varga: grant.bowman@uwyo.edu (G.R. Bowman), krisztina. varga@unh.edu (K. Varga)

https://doi.org/10.1016/j.jmb.2020.09.020

Edited by Richard W. Kriwacki

#### Abstract

The polar organizing protein Z (PopZ) is necessary for the formation of three-dimensional microdomains at the cell poles in *Caulobacter crescentus*, where it functions as a hub protein that recruits multiple regulatory proteins from the cytoplasm. Although a large portion of the protein is predicted to be natively unstructured, in reconstituted systems PopZ can self-assemble into a macromolecular scaffold that directly binds to at least ten different proteins. Here we report the solution NMR structure of PopZ $^{\Delta 134-177}$ , a truncated form of PopZ that does not self-assemble but retains the ability to interact with heterologous proteins. We show that the unbound form of PopZ $^{\Delta 134-177}$  is unstructured in solution, with the exception of a small amphipathic  $\alpha$ -helix in residues M10-117, which is included within a highly conserved region near the N-terminal. In applying NMR techniques to map the interactions between PopZ $^{\Delta 134-177}$  and one of its binding partners, RcdA, we find evidence that the  $\alpha$ -helix and adjoining amino acids extending to position E23 serve as the core of the binding motif. Consistent with this, a point mutation at position I17 severely compromises binding. Our results show that a partially structured Molecular Recognition Feature (MoRF) within an intrinsically disordered domain of PopZ contributes to the assembly of polar microdomains, revealing a structural basis for complex network assembly in Alphaproteobacteria that is analogous to those formed by intrinsically disordered hub proteins in other kingdoms.

© 2020 Elsevier Ltd. All rights reserved.

# Introduction

Biological systems are inherently complex, often involving multistep biochemical pathways and multiple levels of regulation among a large number of physically and functionally interacting components. In many cases, interactive networks are highly dynamic, changing rapidly in response to regulatory signals and adjusting their connectivity to accommodate a range of activities. Interestingly, there is a positive correlation between higher levels of complexity and higher levels of structural disorder in networking

components. <sup>1,2</sup> At the core of these networks are intrinsically disordered proteins (IDPs) and their intrinsically disordered domains (IDDs) that have little or no native structure outside of their interactions with other proteins. Moreover, the disordered nature of the protein binding interface is inherent to the function of dynamic, multi-partner binding interfaces, <sup>3</sup> hereafter referred to as interaction hubs.

In cases where the IDD serves as the hub interface, core interface regions of IDD hubs tend to be 10–50 amino acids in length.<sup>4</sup> The contact sequence on the IDD side of a hub is a conserved region called a Molecular Recognition Feature

0022-2836/© 2020 Elsevier Ltd. All rights reserved.

Journal of Molecular Biology (2020) 432, 6092-6107

(MoRF). A prominent example of an IDD hub protein is the tumor suppressor protein p53, which physically interacts with numerous binding partners via IDDs with MoRFs located in the N- and C-terminal sections of the protein. <sup>5–7</sup> There are a number of other examples of IDD hubs in eukaryotic systems, <sup>8–10</sup> and their inherent networking capability may have been important in supporting the expansion of organismal complexity in this kingdom. <sup>1,11</sup> Furthermore, investigations of IDP structure and function have direct implications for cancer research, as IDPs account for 79% of proteins associated with human cancer. <sup>12</sup>

The structures of IDDs at hub interfaces can be investigated through X-ray crystallography, nuclear magnetic resonance (NMR) spectroscopy, <sup>13–15</sup> and single molecule techniques. <sup>16</sup> These show that the core of the binding interface consists of a short series of amino acids from the IDD, generally less than 20 residues in length, which acquire a relatively constrained structure as they make direct contact with the globular binding partner. The constrained amino acids usually adopt an irregular coiled conformation, but α-helices and β-strands have also been observed at IDD binding interfaces, and these are predicted at frequencies of approximately 20% and 5%, respectively.<sup>17</sup> The structural flexibility of the IDD also gives the core binding region conformational heterogeneity in the bound state, <sup>18–20</sup> allowing the IDD to shift between a range of potential conformations across a dimpled binding energy landscape with no clear minimum, leading to what is called the "fuzzy complex" model.

In a typical bacterial proteome, 6% of the amino acids are predicted to be disordered and as many as 40% of proteins contain an IDD with the general characteristics of a protein interaction motif.<sup>17</sup> Given the observed correlation between Given the observed correlation between organismal complexity and the number of IDDs and IDD hub proteins in a proteome, 1,11,22,23 it is not surprising that IDDs mediate the assembly of complex structures in bacteria. The C-terminal region of FtsZ is an IDD that interacts with at least six other proteins during assembly and closure of the division ring at mid-cell.<sup>24–26</sup> Complex structures are also found at bacterial cell poles. In many species, cell poles are sites for the assembly of flagella, pili, and stalks, <sup>27–30</sup> and they can also serve as locations for multiprotein complexes that regulate chromosome replication and the directionality of chromosome segregation.3 A wellcharacterized example of complex cell pole organization is Caulobacter crescentus, in which at least 100 different proteins are localized to one or both cell poles over the course of the cell cycle.

In C. crescentus and other Alphaproteobacteria, <sup>34,35</sup> a self-assembling pole-localized scaffolding protein called polar organizing protein Z (PopZ) plays a key role in the assembly of polar complexes. <sup>36</sup> In the absence of PopZ, multiple regulatory proteins fail to be recruited to the cell

poles, and chromosomal centromeres fail to dock at their polar destination. <sup>37,38</sup> Because PopZ has the capacity to self-assemble into oligomers and higher ordered structures,39 overproduction of the protein results in expanded scaffolds, which recruit polar regulatory proteins across a larger area of the cell pole. 37,38 PopZ will also assemble into large macromolecular complexes when expressed in Escherichia coli cells, and these structures will selectively recruit co-expressed binding part-ners. 40,41 Thus far, ten different *Caulobacter* proteins have been found to co-assemble with PopZ in this system, and these include cell cycle regulators, mediators of chromosome segregation, and factors associated with cell polarization. Together with additional evidence that supports direct physical interaction, the conclusion is that PopZ is an interaction hub that facilitates the assembly of multiprotein complexes.

The first 133 amino acids of PopZ were predicted to be intrinsically disordered  $^{41}$  and distinct from the C-terminal self-assembly domain.  $^{39}$  The IDD includes a 25 amino acid sequence at the extreme N-terminal that is required for co-assembly with nine of the ten interaction partners identified in E. coli co-expression experiments. Within this N-terminal sequence is a highly conserved stretch of 10–15 amino acids that is predicted to be  $\alpha$ -helical and may function as a MoRE.  $^{39}$ 

In this work, we have utilized solution NMR spectroscopy to determine the major conformational states of the N-terminal 133 amino acids of PopZ (PopZ $^{\Delta 134-177}$ ). Truncation of the Cterminal of PopZ inhibits the formation of higher assembly, thus PopZ $^{\Delta 134-177}$  stays soluble in solution. We have previously shown that this truncated variant is sufficient for interacting with multiple heterologous binding partners, even in the absence of homo-oligomeric assembly.41 NMR analyses reveal a largely disordered protein with an  $\alpha$ -helical region close to the N-terminal. We also characterize the interaction between PopZ and one of its binding partners, a cell cycle regulatory protein called RcdA. 41,45,46 Our analyses revealed that the binding region comprises the N-terminal  $\alpha$ -helix region and a few amino acids proximal to it. Introducing a point mutation in the binding helical region (117A) diminished the binding capacity of PopZ to RcdA. Thus, we conclusively define a MoRF region within PopZ and gain mechanistic insight

### Results

terial hub protein.

# Structure of PopZ $^{\Delta 134\text{-}177}$ by NMR spectroscopy

into the function of this intrinsically disordered bac-

2D and 3D high resolution solution NMR spectra were acquired using a 700 or 800 MHz NMR spectrometer of the truncated PopZ $^{\Delta134-177}$ , which includes the first 133 residues followed by a Leu-Glu linker and 6xHis-tag. All data were processed

using NMRPipe<sup>47</sup> and analyzed using Sparky from NMRFAM.<sup>48</sup> Uniform peak widths and intensities of NMR spectral peaks indicate PopZ<sup>4134–177</sup> was in a stable state necessary for NMR study. The intrinsic disorder of PopZ $^{\Delta 134-177}$  is shown by the 2D  $^{1}$ H- $^{15}$ N HSQC spectrum with the characteristic narrow <sup>1</sup>H chemical shift dispersion typically seen for IDPs (Figure S1), with the exception of sidechain amine and amide resonances from arginine and glutamine residues, respectively. Comparatively, ordered proteins tend to have a wider dispersion of <sup>1</sup>H resonances than proteins without a well-defined fold. <sup>49</sup> The disordered nature of PopZ<sup>Δ134–177</sup> is further supported by the distinct lack of abundance of long-range interactions in <sup>1</sup>H-<sup>15</sup>N NOESY data. Standard triple resonance experiments were performed for protein backbone and sidechain resonance assignments including HNCA, HNcoCA, CBCAcoNH, HNcaCO, HNCACB, CCcoNH, HBHANH, HBHACONH, and HcccoNH. As such, 84.7% of the protein backbone was assigned, including the Leu-Glu linker on the C-terminal of  $PopZ^{\Delta 134-177}$ . For simplicity, the linker residues are referred to as L134 and E135 in assignments. A full list of the assignments, representative strip plot for making assignments, and schematic showing backbone assignment completeness is presented in the Supplemental Information (Table S1, Figures S2 and S3, respectively). Most of the missing assignments were due to the abundance of proline residues, which account for 20% of the  $PopZ^{\Delta 134-177}$  sequence. We were able to obtain partial conformational information on some of the proline residues by calculating the differences between proline  $C\beta$  and  $C\gamma$  chemical shifts. <sup>50</sup> This analysis indicates that 11 of the 25 proline residues are linked to the preceding amino acid by a peptide bond that is in the *trans* conformation. Additionally, we observed a number of low-intensity peaks in the  $^1\text{H-}^{15}\text{N}$ HSQC spectrum that indicate small subpopulations of PopZ  $^{\Delta134-177}$  conformers. Many of the peaks corresponded to residues next to proline, suggesting that these subpopulations are comprised of species with peptide bonds in the cis configuration.

Carbon secondary chemical shifts are known to be strong reporters on secondary structural characteristics. Typically, secondary chemical shifts are defined as the deviation of  $^{13}\text{Ca},\ ^{13}\text{Cl},$  and  $^{13}\text{C}$  (carbonyl) chemical shifts from those that are generated by random coil.  $^{13}\text{C}\beta$  secondary chemical shifts in PopZ^{134-177} spectra showed a continuous range of negative values between N-terminal residues T9-D25, while  $^{13}\text{C}\alpha$  secondary chemical shifts showed a range of positive values in this same region (Figure S4). These data were plotted in a single structural propensity (SSP) plot that indicates a helical motif in this part of the protein (Figure 1(A)). Multiple correlations observed in the  $^{15}\text{N}$ - and  $^{13}\text{C}$ -edited NOESY-HSQC spectra support the existence of this helix (Figure S5)

including 45 sequential (|i-j|=1) and 13 medium-range  $(|i-j| \le 4)$  correlations. Secondary chemical shifts tended to be more randomly oriented in the middle of the sequence (residues 46–100), as expected for an IDP. In the C-terminal region (residues 101–134), we observed a consistent, but small,  $\alpha$ -helical propensity. In applying our data to the structural analysis program Ponderosa-C/S,  $^{53}$  we did not find evidence for a well-defined  $\alpha$ -helix in the C-terminal region, although the consistent pattern of secondary shifts could indicate transient helical character.

We obtained additional information on long-range orientation by measuring Residual Dipolar Coupling (RDC) in axially stretched polyacrylamide gels. We observed mostly negative couplings in the center of the sequence and a cluster of positive couplings in the suspected α-helical binding region, a pattern that is commonly observed for α-helices in this type of analysis. The C-terminal region (residues 100–134) showed weaker couplings that were both positive and negative. We obtained dipolar coupling information for all residues except for 25 proline residues and 20 other residue couplings that could not be measured due to overlapping NH resonances (Figure 1(B) and (C)).

Torsion angle predictions for φ and ψ were generated from TALOS-N (Table S2). Chemical shift assignments, <sup>15</sup>N-NOESY-HSQC and <sup>13</sup>C-NOESY-HSQC peak lists, and RDC restraints were uploaded to Ponderosa-C/S server<sup>53</sup> for structure calculations. The 20 most favored structures were uploaded to the Protein Structure Validation Software<sup>55</sup> suite for validation. Global quality scores were good, and Ramachandran plots from MolProbity found 85.6% of all residues in most favored regions, 9.5% in allowed regions, and 4.9% in disallowed regions. 97.2% of ordered residues were in favored regions. A more detailed analysis of the validation is presented in Table S3. The 20 predicted structures show no other well folded secondary structure elements besides an N-terminal α-helix (M10-I17) (Figure 2).

Additional analysis was carried out using the CIDER (Classification of Intrinsically Disordered Ensemble Regions) server,  $^{56}$  which is generally utilized to calculate and present the various sequence parameters commonly associated with disordered protein sequences. The analysis yielded low values for fraction of charged residues, FCR (0.256) and net charge per residue, NCPR (-0.195). Kappa ( $\kappa$ ), a patterning parameter describing mixing vs. segregation of charged residues in the linear protein sequence was calculated to be 0.202, and omega ( $\Omega$ ), an analogous parameter that takes into consideration prolines,  $^{57}$  was 0.244. The CIDER results indicated that (i) the net charge per residue was generally negative with the exception of a small net positive region close to the N-terminal (Figure S6(A)), (ii) the charged residues are relatively well-mixed with other residues throughout the pro-

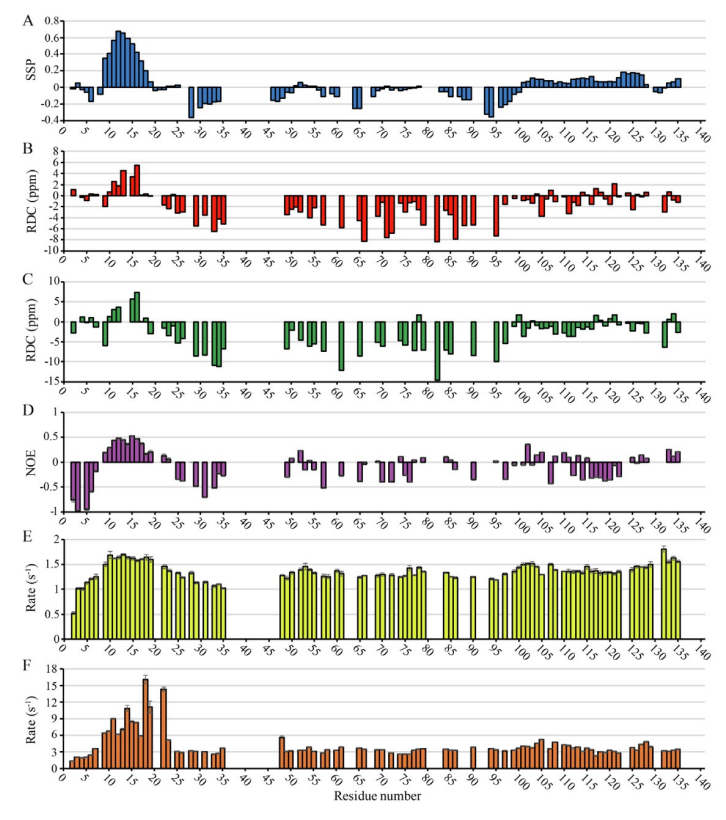


**Figure 1.** NMR characterization of  $PopZ^{\Delta 134-177}$ . (A) Single structure propensity (SSP) plot showing predicted secondary structure domains across the  $PopZ^{\Delta 134-177}$  sequence, where positive values represent helical propensity and negative values represent sheet propensity. (B) and (C) RDC measurements as a function of amino acid residue for a 5.4 mm (B) and 6.0 mm (C) outer diameter (OD) polyacrylamide gel axially stretched to 4.2 mm OD. (D) Heteronuclear NOE ratios observed as a function of amino acid residue. Positive values near the N-terminal are indicative of an ordered secondary structure. (E)  $P_1$  relaxation rates and (F)  $P_2$  relaxation rates observed as a function of amino acid residue. Larger values near the N-terminal are indicative of ordered secondary structure.

tein primary sequence, and (iii) that the proline and charged residues were also well-mixed. The PopZ^134-177 sequence is predicted by CIDER to fall within region 2 of the diagram of states (Figure S6B), the boundary region between weak and strong polyampholytes. The CIDER results are summarized in Table S4.

# Protein dynamics

To obtain information of structure dynamics, we determined hetero NOE ratios (Figure 1(D)) and longitudinal  $(T_1)$  and transverse  $(T_2)$  relaxation

times, as well as their respective  $R_1$  and  $R_2$  relaxation rates (Figure 1(E) and (F), respectively), for the majority of the PopZ^{\Delta134-177} sequence. Global  $T_1$  and  $T_2$  values could not be accurately determined due to the disordered nature of the protein. Hetero NOE values showed primarily small magnitudes of negative sign. However, a range of positive NOE values, typically seen with  $\alpha\text{-helical}$  character, was observed between residues T9 and R19. Additionally, we observed shorter  $T_1$  relaxation times for T9-R19 relative to other residues, and shorter  $T_2$  times across T9-E23 were also

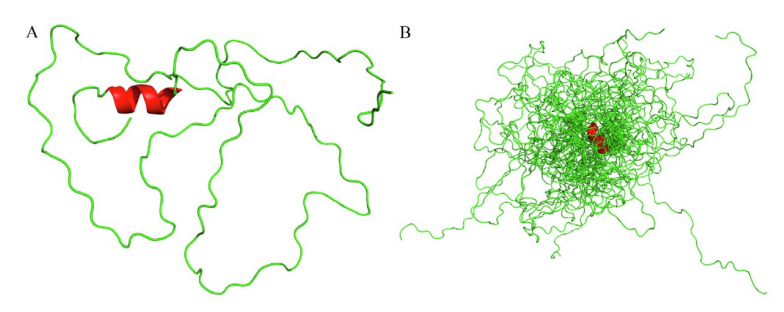


**Figure 2.** PopZ<sup>Δ134-177</sup> structural ensemble. (A) PopZ<sup>Δ134-177</sup> cartoon structure generated from Ponderosa-C/S<sup>53</sup> and visualized using PyMOL.<sup>58</sup> Green represents disorder along the sequence and red represents a short  $\alpha$ -helical secondary structure on the N-terminal. (B) PopZ<sup>Δ134-177</sup> cartoon overlay of the top 20 best-evaluated structures generated from Ponderosa-C/S.<sup>53</sup>

observed, and these local decreases are indicative of  $\alpha\text{-helical}$  character.

# $PopZ^{\Delta 134-177}$ binding studies

We and others have previously shown that PopZ binds to at least ten different binding partners.  $^{41-44}$  Additionally, when  $^{15}$ N-enriched PopZ $^{\Delta134-177}$  was mixed with saturating concentrations of two different unlabeled protein binding partners, we observed that both protein-bound conformations exhibited a nearly identical set of changes in 2D N HSQC spectra. This suggests that PopZ △134-177 interacts with these two binding partners via the same set of amino acids. In this study, we have continued the binding experiments with one of those binding partners, RcdA. In C. crescentus, RcdA is co-localized with PopZ at one of the cell poles at the time of chromosome replication initia-<sup>59</sup> and it serves as an adaptor that interacts with specific protein substrates and links them to the ClpXP protease for degradation *in vitro*<sup>60</sup> and *in vivo*. 44,59 PopZ interaction appears to be functionally separable from protease adaptor activity, suggesting that RcdA has multiple binding interfaces. <sup>61,62</sup> By observing <sup>1</sup>H-<sup>15</sup>N HSQC spectra of isotopically labeled PopZ<sup>Δ134-177</sup> under multiple RcdA concentrations and at a higher magnetic field (700 MHz), we obtained sufficient resolution for accurate peak identification even in congested

regions of the spectra. 2D <sup>1</sup>H-<sup>15</sup>N HSQC spectra were acquired from 130 μM <sup>15</sup>N-enriched PopZ<sup>Δ134-177</sup> in the presence of unlabeled RcdA binding partner at a range of concentrations between 0 and 960 μM (Figure 3 (A) and (B)). Most PopZ<sup>Δ134-177</sup> NMR peaks remained unchanged in all conditions, indicating residues that do not interact with RcdA. For a minority of PopZ<sup>Δ134-177</sup> residues, increasing concentration of RcdA caused chemical shift

perturbation and spectral broadening, and in some cases led to severe signal attenuation or loss of detection. Those peaks that display the greatest shifts and broadening likely indicate residues that interact directly with RcdA, while peaks that display moderate signal attenuation and chemical shift perturbation likely correspond and orientical still perturbation likely correspond to amino acids that participate in secondary or indirect binding interactions. Binding residues were determined by comparing combined ΔHN chemical shifts for each residue, where peaks undergoing a shift greater than the standard deviation were considered binding.<sup>63</sup> Combined AHN lepezies with perturbations (Figure 3/CN) ΔHN chemical shift perturbations (Figure 3(C)) and peak intensity perturbations (Figure S7) of  $PopZ^{\Delta 134-177}$  upon binding to RcdA reveals that the binding motif of  $PopZ^{\Delta 134-177}$  is between T9-E23 (Figures 4 and S8), as peaks corresponding to these residues undergo both significant chemical shift perturbations and line broadening most likely due to direct interaction with RcdA, although potential secondary structure changes cannot be excluded. Residue D25 is expected to experience indirect binding effects, as it exhibits chemical shift perturbation but no significant broadening. Notably, the α-helix (M10-I17) determined by our structural model is found within the RcdA binding region. A schematic of full-sequence PopZ showing secondary structure elements and the proposed binding region is shown in Figure 4(C).
While most perturbed peaks broadened beyond

While most perturbed peaks broadened beyond detection, some peaks were still detectable in the baseline when we significantly lowered the contour levels of the spectra (Figure 3(B)). Residues L14, I21, and S22 are likely binding as well, but their exact chemical shift perturbation could not be determined due to extensive overlap with neighboring peaks. T9 and E23 (residues at the edge of the binding region) showed only a moderate amount of chemical shift perturbation

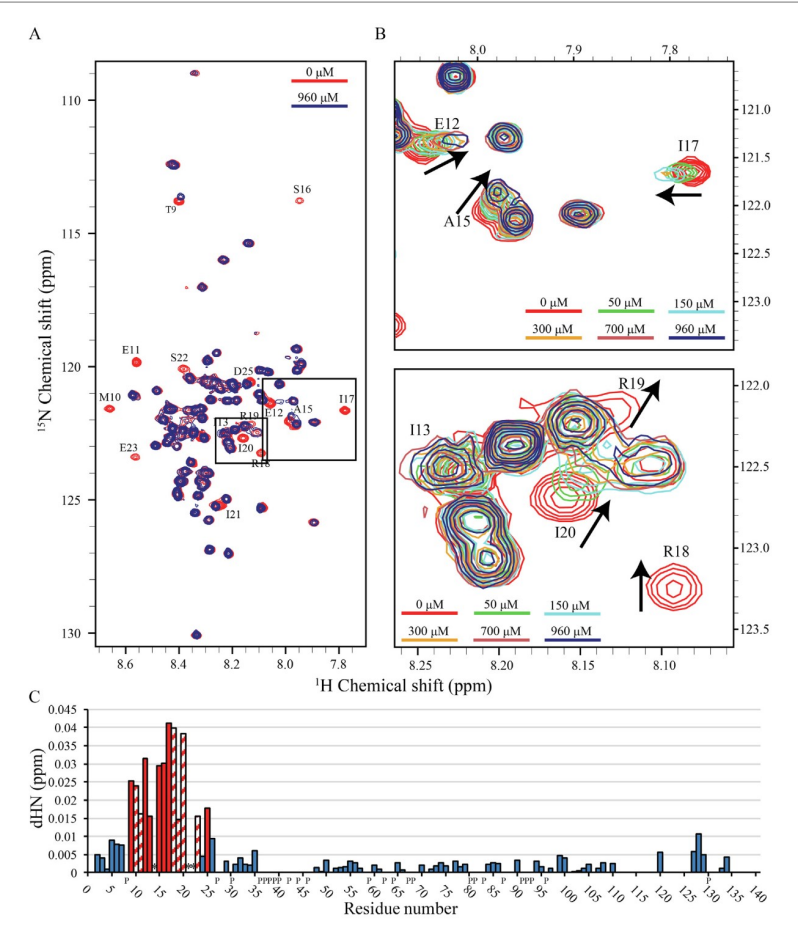
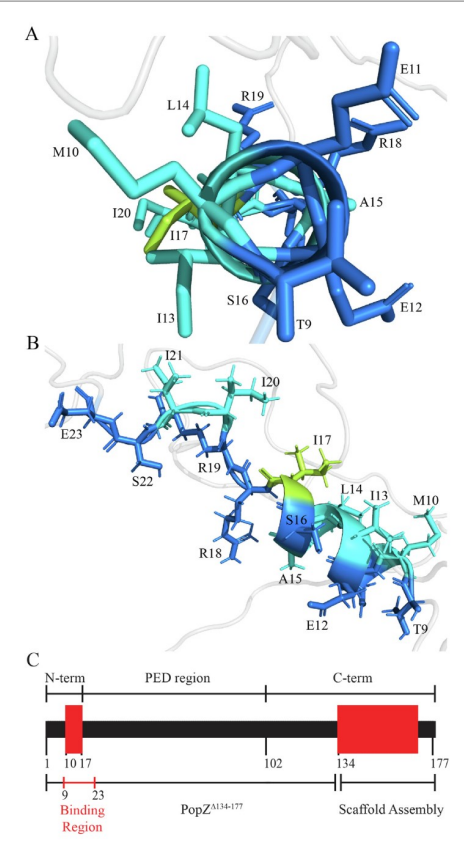


Figure 3. Binding of PopZ<sup>Δ134-177</sup> to RcdA. 2D <sup>1</sup>H-<sup>15</sup>N HSQC spectra overlay of <sup>15</sup>N-enriched PopZ<sup>Δ134-177</sup> in solution with and without the RcdA binding partner exhibit spectral changes upon binding. Colored bars show RcdA concentration for each spectrum. (A) 130 μM PopZ<sup>Δ134-177</sup> with differing concentrations of RcdA: 0 μM (red) and 960 μM (blue). Peaks undergoing significant change are labeled. For simplicity, the spectra were shown without the sidechain region. Dashed boxes represent regions seen in (B). (B) Enlarged regions highlight changes upon increasing RcdA concentration. Arrows indicate direction of peak shift. Binding of RcdA resulted in the chemical shift perturbation and significant broadening of a number of peaks. The contours were lowered in the spectra with high concentration of RcdA to show weak peaks. (C) ΔHN combined chemical shift perturbations of PopZ<sup>Δ134-177</sup> upon binding to RcdA. Binding is indicated by the most pronounced chemical shift perturbations (red) found between residues T9-E23. The patterned columns represent residues that perturbed beyond detection before saturation was achieved. Therefore, the perturbation data from these patterned columns are from the last titration point where the peak was observed. Asterisks indicate residues with significant perturbations that we were not able to determine precisely due to severe peak overlap. "P" labels on the x-axis indicate proline residues which inherently cannot be observed in 2D <sup>1</sup>H-<sup>15</sup>N HSQC spectra. A few resonances in the C-terminal region could not be observed under the buffer conditions for ligand binding experiments.



**Figure 4.** Binding motif of PopZ<sup>Δ134–177</sup>. (A) The amphipathic nature of the helix is shown from this perspective, where hydrophobic residues are colored cyan and hydrophilic residues are colored blue. I17, a critical residue for binding, is colored limon for distinction. Hydrogen atoms have been removed for simplicity. (B) The binding motif as viewed from the side. Structures were generated from Ponderosa-C/S<sup>53</sup> and visualized using PyMOL.<sup>58</sup> (C) Schematic of full sequence PopZ. Secondary structure elements are shown in red and disordered regions are shown in black. Sections are separated to show the N-terminal, proline-glutamate rich domain (PED), C-terminal, binding region, and scaffold assembly region.

and signal broadening, which is likely induced by secondary or indirect binding effects. D24 showed little change. The chemical shift perturbations that we observed in these experiments are closely matched with those produced by another binding partner, ChpT $^{41}$  indicating that the same subset of amino acids in PopZ $^{\Delta 134-177}$  participate in binding to both partners. We therefore conclude that residues T9-E23, which include an  $\alpha$ -helix that spans M10-I17, act as a MoRF region that is directly responsible for interacting with at least two of its binding partners. Similar observations of chemical

shift perturbations have been reported in the bound conformations of other MoRFs, including one in the C-terminal domain of p53. $^{9,64,65}$  Interestingly, CIDER results indicated that the net charge per residue across the PopZ $^{\Delta134-177}$  sequence is generally negative with the exception of a small net positive region in the MoRF region due to residues R18 and R19 (Figure S6(A)). This could suggest that the dispersion of positive and negative charge within the binding region is critical for the electrostatic interaction between PopZ and its protein binding partners.

To obtain genetic evidence for the functionality of the predicted MoRF in PopZ^{A134-177}, we introduced a point mutation into the most highly conserved residue within the T9-E23 region by replacing lle 17 with Ala (I17A). Notably, the  $^1\text{H}^{-15}\text{N}$  HSQC spectral peaks corresponding to the  $\alpha\text{-helix}$  were perturbed compared to wildtype PopZ^{A134-177} spectra, indicating the I17A mutation disrupts the binding site. Adding excess RcdA (up to 1.0 mM) to 120  $\mu\text{M}$  I17A PopZ^{A134-177} did not induce spectral shifts or broadening (Figure S9), indicating that binding did not occur. This indicates that I17 of PopZ^{A134-177} is critical for binding RcdA in vitro. We also tested RcdA binding in an E. coli co-expression assay (Figure 5). Here, RcdA was produced as a fusion protein with green fluorescent protein (RcdA-GFP) and co-expressed with either full-length wildtype PopZ or the full-length I17A mutant (each produced as fusions with mCherry for visualization by fluorescence microscopy). Due to the presence of the C-terminal self-assembly domain in full-length PopZ, both of the PopZ variants accumulated at the cell poles of the bacteria. RcdA-GFP exhibited strong co-localization with wildtype PopZ, but much weaker co-localization with the I17A mutant, confirming the interaction defeat.

# **Discussion/Conclusion**

In this work, we have structurally characterized the multi-protein binding domain of the alphaproteobacterial hub protein PopZ. Native PopZ is 177 amino acid residues in length, and we have investigated a truncated version,  $PopZ^{\Delta 134-177}$ , which includes the first 133 residues, a short linker, and 6xHis-tag. In the unbound form of PopZ $^{\Delta 134-177}$ , we find that the critical binding motif includes a short  $\alpha$ -helical segment between residues M10 and I17, with additional unstructured residues on either side. To analyze a bound form of PopZ<sup>A134-177</sup> and probe the binding interface, we used NMR titration studies against a binding partner, RcdA. We found that residues T9-E23 bind either directly or indirectly to the RcdA, forming a MoRF that may include a mixture of  $\alpha$ -helical and coiled features. Residue I17, which lies at the center of the binding motif, remains critical for the interaction, and disruption of this residue leads to significant perturbation of the MoRF spectral peaks and drastic loss in binding. Adjacent to I17 lie R18 and R19, which contrast with the generally negative charge of PopZ $^{\Delta 134-177}$  in forming a small island of positive charge. Positive charges at these positions are evolutionarily conserved and are

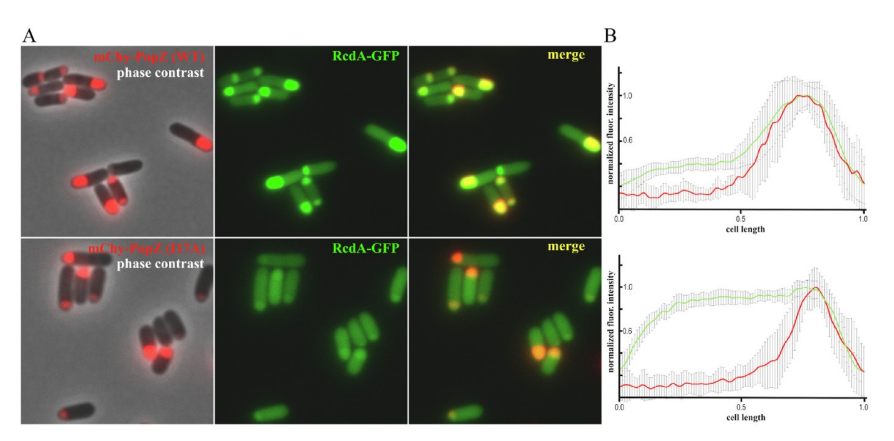


**Figure 5.** Localization of RcdA-GFP and wildtype or I17A mutant PopZ in an  $E.\ coli$  co-expression assay. (A) Full-length wildtype PopZ (upper panels) or the I17A point mutant (lower panels) was fused to the C-terminal of mChy (red signal) and co-expressed in  $E.\ coli$  cells with RcdA-GFP (green signal). Single channel fluorescence images are overlayed on a phase contrast image (left panels), shown independently (center panels), or overlayed to show co-localization of fluorescent proteins (right panels). (B) Distributions of mChy-PopZ and RcdA-GFP are shown by plotting normalized fluorescent pixel intensities (Y-axis) as a function of cell length (X-axis), with cells oriented such that 0 marks open poles and 1 marks poles with mChy-PopZ foci (n=10). Bars show standard deviation between cells.

likely to be important for electrostatic interactions between PopZ and its binding partners. Consistent with this, changing R19 to glutamate contributes to the loss of binding affinity to ParA and ParB. 66

In earlier work we used NMR spectroscopy to demonstrate binding between PopZ<sup>A134-177</sup> and a different binding partner, ChpT.<sup>41</sup> Comparison of the spectra from RcdA and ChpT binding showed a nearly identical pattern of chemical shift perturbations, suggesting that both proteins interact with the same set of amino acids in PopZ<sup>A134-177</sup>, even though these two proteins exhibit no sequence or structural homology.<sup>62,67</sup> The only significant difference was in the peak corresponding to D25, located at the C-terminal end of the binding region, which did not show significant perturbation in complex with ChpT.

The cell cycle-dependent timing and intensity of polar localization of PopZ binding partners differ significantly and are not directly proportional to the localization pattern of PopZ. The transmembrane scaffolding protein SpmX is recruited by PopZ to the stalked pole, 43 whereas transmembrane histidine kinases DivL and CckA, which are also direct binding partners of PopZ, are localized to the opposing swarmer pole or distributed between the two poles, respectively.6 Other PopZ binding partners, including RcdA, ChpT and the protease adaptor protein CpdR,69 are localized transiently to the stalked pole. Such wide variation in timing and localization of PopZ binding partners could not occur if polar localization were determined simply by the ability to interact with PopZ, and this suggests the existence of regulatory mechanisms that affect PopZ interaction. Kinases, their downstream effectors, and other factors that regulate the production and degradation of the secondary messenger c-di-GMP exhibit highly polarized localization and activity in C. crescentus. PopZ binds directly to some of the elements within these signaling networks, and in doing so it could establish feedback loops that reinforce polar asymmetry through a signal that increases or decreases PopZ's affinity for certain binding partners. Protein phosphorylation is one potential signal, as interactions involving eukaryotic IDPs can be regulated in this manner.<sup>73–75</sup> The symmetry-break in *C. cres*- $^{-75}$  The symmetry-break in  $reve{C}$ . crescentus could be established by cell division, if the PopZ that accumulates at the newly formed pole establishes different signaling complexes than PopZ at the old pole.

We have shown that the PopZ side of the binding interface includes an  $\alpha$ -helix. Binding helices are common in eukaryotic IDP hub domains, and there are multiple examples of interactions that are mediated by a single helix.  $^{76-79}$  In many IDPs, relatively stable elements of secondary structure called  $\alpha MoRFs$  form the core of the binding interace, and these are thought to aid binding by providing pre-formed structure that increases the stability

of the bound complex.<sup>80–82</sup> Our structural analysis of PopZ<sup>Δ134-177</sup> demonstrates an αMoRE in demonstrates an aMoRF in Alphaproteobacteria, a feature that appears to be less common in bacterial proteomes than in eukary-otic proteomes.<sup>17</sup> Another bacterial protein with Another bacterial protein with comparable structural and functional qualities is the divisome assembly protein FtsZ, which has a C-terminal IDP hub domain consisting of a disordered linker followed by a MoRF. In complex with different binding partners, FtsZ's MoRF region can be partially  $\alpha$ -helical<sup>25,83</sup> or an extended linear motif.26 For FtsZ, a destabilized αMORF may provide increased structural flexibility that allows binding to a wider range of binding surfaces. While our results suggest that the MoRF in PopZ is  $\alpha$ -helical, transient unfolding is likely to occur, and some binding complexes may utilize other structural conformations of this region.8

Since our analysis of secondary structure was limited to the unbound state of  $PopZ^{\Delta 134-177}$ , a remaining question is whether the helical region in the N-terminal MoRF of PopZ $^{\Delta 134-177}$  is altered upon interaction with binding partner proteins. For some IDPs, the transition from unbound to bound state involves the formation of additional  $\alpha$ helices, 85 extension of a preformed helix, 86 or stabilization of coil. 87 Similarly, the bound form of PopZ <sup>∆</sup>134-177 could acquire more complex structural character through stabilization of features on either side of the M10-I17 helix. Consistent with this, we find that the set of amino acids that undergo chemical shift perturbation during interaction extends out to residue D25 for RcdA or E23 for ChpT. We note that M10-I17 forms an amphipathic helix (Figure 4A), and that the amphipathic nature of this structure would continue if the helix were extended to E23. Furthermore, secondary structural prediction algorithms consistently predict that the helix extends to at least I21 or S22. 46,88 Together, the evidence suggests that the helical portion of the PopZ  $^{\Delta}$ 134-177  $^{\alpha}$ MORF could include several amino acids beyond I17 in the bound form of PopZ $^{\Delta}$ 134-177 though form , though further studies will be needed to confirm this hypothesis.

Our finding that the I17A mutation inhibits the interaction between PopZ and RcdA is consistent with earlier studies, which show that cell division defects in a *popZ* deletion strain can be rescued by expression of wildtype PopZ. The I17A mutant cannot rescue the cell division defects in a *popZ* deletion strain, and the I17A mutant PopZ protein fails to recruit a direct binding partner, SpmX, to the cell pole.<sup>39,43</sup> Similarly, PopZ bearing an I13A point mutation was found to be partially functional in rescuing *popZ* deletion phenotypes. We propose that the hydrophobic side of the amphipathic PopZ αMoRF (which includes I13 and I17) fits into a hydrophobic groove on RcdA, ChpT, SpmX, and other binding partners, in a manner that is analogous to the interaction of the amphipathic PUMA αMoRF with McI-1.<sup>78</sup> Hydrophobic residues have

been shown to increase binding affinity in MoRF regions, <sup>89</sup> as demonstrated for PUMA<sup>90</sup> and other binding helices in IDPs. <sup>91,92</sup> Mutations in charged and polar amino acids in the N-terminal region of PopZ appear to have variable effects on binding. For example, the E12K R19E double mutation inhibits binding to ParB but not ParA, while the S22P mutant inhibits binding to ParA but not ParB. <sup>66</sup> It may be that all or most of PopZ's binding partners use contact with the hydrophobic side of the helix formed by M10-I17 to form a "fuzzy" binding intermediate, <sup>21</sup> but that these interactions are not strong enough to lead to longer-term binding without additional contacts on other faces of the helix or peripheral contacts outside of the core helix.

In light of the fact that PopZ forms trimers, hexamers, and higher ordered structures in vivo, <sup>39,46</sup> it is also possible that multiple M10-I17 + MoRF helices work together to form a complex interface that binds the target protein. Although our results do not rule this model out, we note that our data was collected with a truncated form of PopZ that does not self-assemble.35 question is how the large, ~80 amino acid disordered region on the C-terminal side of the αMoRF region of PopZ contributes to binding. While total deletion of the disordered region results in loss of PopZ function, it can be reduced to half size and also scrambled without having strong effects on the ability to interact with other proteins<sup>41</sup> or complement the popZ knockout phenotype in vivo. This region may be a flexible linker that separates the PopZ C-terminal oligomerization domain (residues 134-177) from the MoRF, while also contributing to the structural disorder that facilitates "fuzzy complexes" between IDP and target proteins. $^{21,93}$  We suggest that PopZ $^{\Delta134-177}$  binds and reels the binding partners to the superstructure through sampling of its various disordered conformers, where a wide range of motion increases the likelihood of encountering and binding to other proteins in its local environment. This is similar to the fly-caster model for other IDPs, <sup>94</sup> although there is no clear evidence to suggest that PopZ would fold upon binding. Oligomerization of full-length PopZ via the C-terminal domain, which is predicted to be highly structured, may act as an anchor around which these binding events occur. Another possibility that is not mutually exclusive is that the disordered domain creates a phase-separated droplet,95 and this may provide a microenvironment that is conducive to hub binding activity, as has been proposed for the organization of transcription factor complexes in eukarvotes.

# **Materials and Methods**

# $\text{PopZ}^{\Delta 134\text{-}177}$ and RcdA protein expression and purification for NMR experiments

The expression and purification of  $PopZ^{\Delta 134-177}$  protein was described previously.<sup>41</sup> Briefly, wild-

type PopZ<sup>Δ134-177</sup> was cloned into the *E. coli* expression vector pET28a (Novagen) with a 6xHis-tag and Leu-Glu linker (strain YA#134), see Table S5. U-<sup>15</sup>N and U-<sup>13</sup>C, <sup>15</sup>N enriched variants of PopZ<sup>Δ134-177</sup> were produced by expressing the proteins in minimal media supplemented either with <sup>15</sup>NH<sub>4</sub>Cl (for uniform labeling with nitrogen-15) or <sup>15</sup>NH<sub>4</sub>Cl and <sup>13</sup>C<sub>6</sub>-glucose (for uniform labeling with nitrogen-15 and carbon-13), respectively. A plasmid carrying the PopZ<sup>Δ134-177</sup> gene with the 117A mutation was also constructed (strain YA#129), see Table S5. U-<sup>15</sup>N enriched I17A PopZ<sup>Δ134-177</sup> were expressed in minimal medium supplemented with <sup>15</sup>NH<sub>4</sub>Cl. Isotopes were purchased from Cambridge Isotope Laboratories, Inc.
PopZ<sup>Δ134-177</sup> was expressed for 12 h by shaking

PopZ<sup>Δ134-17</sup> was expressed for 12 h by shaking at 37 °C after induction. Cell pellets were resuspended in Buffer A (25 mM Tris, 150 mM NaCl, 20 mM imidazole at pH 7.5) supplemented with Halt EDTA-free protease inhibitor and Benzonase nuclease. The cells were lysed using a French press. The protein was purified by two rounds of Ni-affinity chromatography using a Fast Protein Liquid Chromatography instrument (FPLC; GE Healthcare AKTA purifier 900 equipped with GE Healthcare HisTrap HP 1 ml column). The protein fractions were pooled and the buffer was exchanged to Buffer B (25 mM Tris, 150 mM NaCl pH 7.5). The purity of the sample was analyzed by 12% SDS-PAGE and staining with Coomassie blue.

The expression and purification of the RcdA protein was described previously.<sup>41</sup> In short, natural abundance SUMO-RcdA fusion protein was expressed in E. coli by shaking the cells in LB medium for 12 h at 21 °C after induction. Cell pellets were resuspended in Buffer C (20 mM HEPES, 100 mM KCl, 2 mM MgCl2, 20 mM imidazole at pH 7.5). Cells were lysed using a French press and the protein was purified by two rounds of Niaffinity chromatography using FPLC. The protein was buffer exchanged into Buffer D (25 mM Tris, 150 mM NaCl at pH 7.5), and the fusion protein was cleaved by 1 Unit SUMO Express Protease (Lucigen) per 200 μg Sumo-RcdA. After cleavage, the protein samples were purified by Ni-affinity chromatography using FPLC. The protein was buffer exchanged to Buffer E (20 mM HEPES, 100 mM KCI, 2 mM MgCl<sub>2</sub> at pH 7.5) for NMR experiments. The purity of the samples was analyzed by 12% SDS-PAGE and staining with Coomassie blue.

#### NMR spectroscopy

For NMR assignment experiments, the purified PopZ^{\Delta134-177} was buffer exchanged into Buffer F (50 mM phosphate, 50 mM citric acid, 20 mM NaCl, and 3 mM NaN $_3$  at pH 5.5). D $_2$ O, NaN $_3$ , and DSS were added to a 5% v/v, 4 mM, and 0.2 mM final concentration, respectively, at a final PopZ^{\Delta134-177} concentration of 0.90 mM. The protein concentration was estimated using UV–Vis

spectrophotometry ( $\varepsilon_{280} = 2980~{\rm cm}^{-1}~{\rm M}^{-1}$ ). The NMR sample was packed into a 5-mm Shigemi NMR tube. The 2D <sup>1</sup>H-<sup>15</sup>N Heteronuclear Single Quantum Correlation (HSQC) NMR spectrum and standard protein backbone and side-chain NMR spectra (including 3D HNCA, HNCoCA, HNCO, HNCaCO, HNCACB, CBCAcoNH, CCcoNH, HBHANH, HBHAcoNH, and HcccoNH, <sup>15</sup>N- and <sup>13</sup>C-edited NOESY) were collected at 25 °C on a Bruker AVANCE III HD 800 MHz NMR spectrometer (CUNY Advanced Science Research Center, New York, NY) equipped with a 5-mm triple resonance inverse TCl CryoProbe. All NMR data were processed using NMRPipe.<sup>47</sup> Analysis and assignments of the 2D and 3D data sets were carried out using NMHFAM-Sparky. The document process was facilitated by using the PINE ser-ment process was facilitated by using the PINE ser-ment process was facilitated by using the PINE ser-ment process was facilitated by using the PINE ser-ser process was facilitated by using the PINE ser-ser process was facilitated by using the PINE ser-ser process was facilitated by using the PINE ser-per process was facilitated assignments. completing the assignments manually. The secondary chemical shift values were calculated by subtracting experimental chemical shift values from random coil values supplied by NMRFAM-Sparky. Relaxation and heteronuclear NOE data were analyzed using the Dynamics Center software package (Bruker BioSpin, Inc).

To characterize the binding site of PopZ $^{\Delta 134-177}$  to RcdA, a series of 130 µM  $^{15}$ N-enriched PopZ $^{\Delta 134-177}$  samples were prepared in the presence of varying concentration of RcdA in Buffer E: 0 µM RcdA (PopZ $^{\Delta 134-177}$  only), 50 µM RcdA, 100 µM RcdA, 150 µM RcdA, 200 µM RcdA, 300 µM RcdA, 500 µM RcdA, 200 µM RcdA, 900 µM RcdA, 900 µM RcdA, and 960 µM RcdA. 2D  $^{1}$ H- $^{15}$ N HSQC spectra were collected on all samples at 25  $^{\circ}$ C on a Bruker AVANCE III HD 700 MHz NMR spectrometer (CUNY Advanced Science Research Center, New York, NY). Combined  $^{1}$ H and  $^{15}$ N chemical shift perturbations ( $^{\Delta}$ HN) were calculated using Eq. (1),

$$\Delta HN = \sqrt{(\Delta H)^2 + (0.15 \times \Delta N)^2}$$
 (1)

where  $\Delta H$  and  $\Delta N$  are the chemical shift perturbations in ppm for  $^1H$  and  $^{15}N$ , respectively, and 0.15 is a scaling factor corresponding to the relative chemical shift dispersion in the  $^1H$  and  $^{15}N$  dimensions.

# Residual dipolar coupling (RDC)

For RDC NMR experiments, the purified PopZ<sup>A134-177</sup> was buffer exchanged into Buffer F. The protein was concentrated and D<sub>2</sub>O, NaN<sub>3</sub>, and DSS were added to a 5% v/v, 4 mM, and 0.2 mM concentration, respectively, at a final PopZ<sup>A134-177</sup> concentration of 0.20 mM. The protein sample was used to rehydrate a 5.4 mm or 6.0 mm (outer diameter) gel previously cast and dehydrated (see RDC gel preparation below). The gel was stretched into a New Era Enterprises 4.2 mm (inner diameter) NMR tube for RDC NMR experiments. The <sup>1</sup>H-<sup>15</sup>N HSQC NMR spectrum was collected at 25 °C on a Bruker AVANCE III

HD 800 MHz NMR spectrometer equipped with a 5-mm triple resonance inverse TCI CryoProbe.

#### **RDC** gel preparation

RDC gel preparation and sample preparation were performed using New Era Enterprises gel kits. A 5.4% acrylamide RDC gel was created by mixing 40% bis-acrylamide purchased from Bio-Rad with water and polymerized with 0.1% w/v ammonium persulfate and 0.1% v/v TEMED. This was cast in a New Era Enterprises gel stretching chamber and allowed to polymerize overnight at room temperature with the chamber sealed with parafilm to prevent leakage. The gel was removed from the chamber and dialyzed in pure water for 8 h followed by a second round of dialysis in fresh water. The gel was then cut to approximately 2.1 cm in length using a razor blade and then dehydrated on a flat surface for 18-24 h in a desiccator at room temperature. The dehydrated gel was placed back in the gel chamber and the gel was incubated overnight with the protein solution at 4 °C before being stretched into a New Era Enterprises 4.2 mm (inner diameter) NMR tube using a New Era Enterprises gel stretching kit. The end of the gel was slowly pressed out of the tube until approximately 2.1 cm in length was left in the tube. The protruding section of the gel was cut off using a razor blade.

#### Structural constraints

Backbone angles and secondary structure elements were predicted using TALOS-N. 99 Xplor-NIH based calculations from the Ponderosa-C/S package<sup>53</sup> calculated the conformational states with the Ponderosa-X refinement option which utilized chemical shift values, distance constraints from <sup>1</sup>H-<sup>15</sup>N HSQC NOESY and <sup>1</sup>H-<sup>13</sup>C HSQC NOESY spectra, and residual dipolar coupling (RDC) constraints. 100 Weighting factors were kept at default values. Tolerance levels were set at 0.35, 0.35, and 0.025 ppm for N, C, and H, respectively. Constraint violations from the top 20 bestevaluated structures were analyzed using Pon-derosa Analyzer<sup>48,53</sup> and structural calculations were subsequently refined in iterative steps using the Constraints only-X option. Finally, an ensemble of 100 conformers was calculated using the final step option with a following explicit water refinement force field by Xplor-NIH. <sup>101</sup> The explicit water refinement consisted of the following steps: (1) immersion in a shell of water (7 Å) and energy minimization; (2) slow heating from 100 to 500 K in 100 K temperature steps with 200 molecular dynamics (MD) steps per temperature step with 3 fs time steps; (3) refinement at 500 K using 2000 MD steps with 4 fs time steps; (4) slow cooling from 500 K to 25 K in 25 K temperature steps with 200 MD steps per temperature step with 4 fs time steps; (5) 200 steps for final energy minimization. 102 The 20 best evaluated structures were submitted to the Protein Structure Validation Software (PSVS)<sup>55</sup> suite for structural validation.

# **CIDER** analysis

Sequence analysis of  $PopZ^{\Delta 134-177}$  (without the Leu-Glu linker and 6xHis-tag) was performed by accessing CIDER<sup>56</sup> at http://pappulab.wustl.edu/CIDER/analysis/.

#### Fluorescence microscopy

Overnight cultures of E. coli bearing plasmids pACYC + mCherry-PopZ (or pACYC + mCherry-PopZ I17A) and pBAD + RcdA-GFP (strain YA#138, YA#142, see Table S5) were diluted 100fold in fresh LB media and grown for 2 h at 30 °C before stimulation of mChy-PopZ and RcdA-GFP expression with 100  $\mu$ M IPTG and 0.005% arabinose, respectively. For induction of pACYC + mCherry-PopZ I17A, 140  $\mu$ M IPTG was added to keep the expression equivalent to pACYC + mCherry-PopZ expression. Cells were immobilized on a 1% agarose gel pad and viewed with a Zeiss Axio Imager Z2 epifluorescence microscope equipped with a Hamamatsu Orca-Flash 4.0 sCMOS camera and a Plan-Apochromat 100x/1.46 Oil Ph3 objective. Zen Blue software was used for image capture and quantification. Ten representative cells from WT and I17A mutant PopZ samples were chosen. Cells with mChy-PopZ foci at both poles were excluded. Pixel intensities (after subtracting background fluorescence) average measured along a straight line drawn lengthwise through the middle of the cells. Cubic spline interpolation was used to generate fluorescence intensity values for 100 equally spaced points on each line, and pixel intensities were normalized to 1 as the maximum value.

# **Accession numbers**

BMRB ID: 30773; PDB ID: 6XRY.

# CRediT authorship contribution statement

Christopher T. Nordyke: Investigation, Formal analysis, Validation, Visualization, Writing original draft, Writing - review & editing. Yasin Ahmed: Investigation, Formal analysis, Data curation Ryan Z. Puterbaugh: Investigation, Formal analysis, Data curation, Visualization, Writing - original draft, Writing - review & editing. Grant R. Bowman: Conceptualization, Methodology, Formal analysis, Resources, Writing - original draft, Writing - review & editing, Supervision, Project administration, Funding acquisition. Krisztina Varga: Conceptualization,

Methodology, Formal analysis, Resources, Writing - original draft, Writing - review & editing, Supervision, Project administration.

#### Acknowledgements

This project was supported in part by a grant from the National Institute of General Medical Sciences (1R01GM118792) at the National Institutes of Health, the National Science Foundation Major Research Instrumentation Award (DBI-1828319), and the University of New Hampshire startup funds. We would also like to thank Dr. James Aramini at CUNY Advanced Science Research Center (ASRC) for data collection.

#### **Declaration of Competing Interest**

The authors declare that they have no known competing financial interests or personal relationships that could have appeared to influence the work reported in this paper.

# Appendix A. Supplementary material

Supplementary data to this article can be found online at https://doi.org/10.1016/j.jmb.2020.09.020.

Received 16 July 2020; Accepted 25 September 2020; Available online 12 October 2020

#### Keywords:

NMR spectroscopy;
PopZ;
intrinsic disorder;
molecular recognition feature;
hub protein

# Abbreviations:

NMR, nuclear magnetic resonance; PopZ, polar organizing protein Z; IDPs, intrinsically disordered proteins; IDD, intrinsically disordered domains; MoRF, molecular recognition feature; RDC, residual dipolar coupling; PSVS, protein structure validation software; CIDER, classification of intrinsically disordered ensemble regions; NPCR, net charge per residue; FCR, fraction of charged residues

# References

- Yruela, I., Oldfield, C.J., Niklas, K.J., Dunker, A.K., (2017). Evidence for a strong correlation between transcription factor protein disorder and organismic complexity. *Genome Biol. Evol.*, 9, 1248–1265.
- Babu, M.M., (2016). The contribution of intrinsically disordered regions to protein function, cellular

- complexity, and human disease. *Biochem. Soc. Trans.*, **44**, 1185–1200.
- Cumberworth, A., Lamour, G., Babu, M.M., Gsponer, J., (2013). Promiscuity as a functional trait: intrinsically disordered regions as central players of interactomes. *Biochem. J.*, 454, 361–369.
- Malhis, N., Jacobson, M., Gsponer, J., (2016). MoRFchibi SYSTEM: software tools for the identification of MoRFs in protein sequences. *Nucleic Acids Res.*, 44, W488–W493.
- Furth, N., Aylon, Y., Oren, M., (2018). p53 shades of Hippo. Cell Death Differ., 25, 81–92.
- Grossman, S.R., (2001). p300/CBP/p53 interaction and regulation of the p53 response. Eur. J. Biochem., 268, 2773–2778.
- Uversky, V.N., (2016). p53 proteoforms and intrinsic disorder: an illustration of the protein structure-function continuum concept. Int. J. Mol. Sci., 17
- Nyqvist, I., Andersson, E., Dogan, J., (2019). Role of conformational entropy in molecular recognition by TAZ1 of CBP. J. Phys. Chem. B, 123, 2882–2888.
- O'Shea, C., Staby, L., Bendsen, S.K., Tidemand, F.G., Redsted, A., Willemoes, M., et al., (2017). Structures and short linear motif of disordered transcription factor regions provide clues to the interactome of the cellular hub protein radical-induced cell death. J. Biol. Chem., 292, 512–527.
- Jespersen, N., Estelle, A., Waugh, N., Davey, N.E., Blikstad, C., Ammon, Y.C., et al., (2019). Systematic identification of recognition motifs for the hub protein LC8. Life Sci. Alliance, 2
- Nagulapalli, M., Maji, S., Dwivedi, N., Dahiya, P., Thakur, J. K., (2016). Evolution of disorder in mediator complex and its functional relevance. *Nucleic Acids Res.*, 44, 1591– 1612
- De Biasio, A., Ibanez de Opakua, A., Cordeiro, T.N., Villate, M., Merino, N., Sibille, N., et al., (2014). p15PAF is an intrinsically disordered protein with nonrandom structural preferences at sites of interaction with other proteins. *Biophys. J.*, 106, 865–874.
- Delaforge, E., Kragelj, J., Tengo, L., Palencia, A., Milles, S., Bouvignies, G., et al., (2018). Deciphering the dynamic interaction profile of an intrinsically disordered protein by NMR exchange spectroscopy. J. Am. Chem. Soc., 140, 1148–1158.
- Mollica, L., Bessa, L.M., Hanoulle, X., Jensen, M.R., Blackledge, M., Schneider, R., (2016). Binding mechanisms of intrinsically disordered proteins: theory, simulation, and experiment. Front. Mol. Biosci., 3
- Schneider, R., Blackledge, M., Jensen, M.R., (2019). Elucidating binding mechanisms and dynamics of intrinsically disordered protein complexes using NMR spectroscopy. Curr. Opin. Struct. Biol., 54, 10–18.
- Melo, A.M., Coraor, J., Alpha-Cobb, G., Elbaum-Garfinkle, S., Nath, A., Rhoades, E., (2016). A functional role for intrinsic disorder in the tau-tubulin complex. *Proc. Natl. Acad. Sci. U. S. A.*, 113, 14336–14341.
- Yan, J., Dunker, A.K., Uversky, V.N., Kurgan, L., (2016).
   Molecular recognition features (MoRFs) in three domains of life. *Mol. BioSyst.*, 12, 697–710.
- Toto, A., Camilloni, C., Giri, R., Brunori, M., Vendruscolo, M., Gianni, S., (2016). Molecular recognition by templated folding of an intrinsically disordered protein. *Sci. Rep.*, 6
- Had i, S., Mernik, A., Podlipnik, ., Loris, R., Lah, J., (2017). The thermodynamic basis of the fuzzy interaction

- of an intrinsically disordered protein. *Angew. Chem. Int. Ed. Engl.*, **56**, 14494–14497.
- Schwarten, M., Sólyom, Z., Feuerstein, S., Aladağ, A., Hoffmann, S., Willbold, D., et al., (2013). Interaction of nonstructural protein 5A of the hepatitis C virus with SRC homology 3 domains using noncanonical binding sites. *Biochemistry*, 52, 6160–6168.
- Fuxreiter, M., (2019). Fold or not to fold upon binding does it really matter?. Curr. Opin. Struct. Biol., 54, 19–25.
- Schad, E., Tompa, P., Hegyi, H., (2011). The relationship between proteome size, structural disorder and organism complexity. *Genome Biol.*, 12, R120.
- Dosztányi, Z., Chen, J., Dunker, A.K., Simon, I., Tompa, P., (2006). Disorder and sequence repeats in hub proteins and their implications for network evolution. *J. Proteome Res.*, 5, 2985–2995.
- Ortiz, C., Natale, P., Cueto, L., Vicente, M., (2016). The keepers of the ring: regulators of FtsZ assembly. FEMS Microbiol. Rev., 40, 57–67.
- Schumacher, M.A., Huang, K.-H., Zeng, W., Janakiraman, A., (2017). Structure of the Z ring-associated protein, ZapD, bound to the C-terminal domain of the tubulin-like protein, FtsZ, suggests mechanism of Z ring stabilization through FtsZ cross-linking. J. Biol. Chem., 292, 3740– 3750.
- Schumacher, M.A., Zeng, W., (2016). Structures of the nucleoid occlusion protein SImA bound to DNA and the Cterminal domain of the cytoskeletal protein FtsZ. Proc. Natl. Acad. Sci. U. S. A., 113, 4988–4993.
- Mignolet, J., Panis, G., Viollier, P.H., (2018). More than a Tad: spatiotemporal control of Caulobacter pili. Curr. Opin. Microbiol., 42, 79–86.
- Ardissone, S., Viollier, P.H., (2015). Interplay between flagellation and cell cycle control in Caulobacter. *Curr. Opin. Microbiol.*, 28, 83–92.
- Kazmierczak, B.I., Schniederberend, M., Jain, R., (2015). Cross-regulation of Pseudomonas motility systems: the intimate relationship between flagella, pili and virulence. *Curr. Opin. Microbiol.*, 28, 78–82.
- Ringgaard, S., Yang, W., Alvarado, A., Schirner, K., Briegel, A., (2018). Chemotaxis arrays in Vibrio species and their intracellular positioning by the ParC/ParP system. J. Bacteriol., 200, e00793—e817.
- Ramachandran, R., Jha, J., Chattoraj, D.K., (2014). Chromosome segregation in Vibrio cholerae. *J. Mol. Microbiol. Biotechnol.*, 24, 360–370.
- Kloosterman, T.G., Lenarcic, R., Willis, C.R., Roberts, D. M., Hamoen, L.W., Errington, J., et al., (2016). Complex polar machinery required for proper chromosome segregation in vegetative and sporulating cells of Bacillus subtilis. *Mol. Microbiol.*, 101, 333–350.
- Werner, J.N., Chen, E.Y., Guberman, J.M., Zippilli, A.R., Irgon, J.J., Gitai, Z., (2009). Quantitative genome-scale analysis of protein localization in an asymmetric bacterium. Proc. Natl. Acad. Sci. U. S. A., 106, 7858– 7863
- Grangeon, R., Zupan, J., Jeon, Y., Zambryski, P.C., (2017). Loss of PopZ(At) activity in agrobacterium turnefaciens by deletion or depletion leads to multiple growth poles, minicells, and growth defects. *Mbio*, 8
- Pfeiffer, D., Toro-Nahuelpan, M., Bramkamp, M., Plitzko, J. M., Schuler, D., (2019). The polar organizing protein PopZ is fundamental for proper cell division and segregation of

- cellular content in magnetospirillum gryphiswaldense. Mbio. 10
- Berge, M., Viollier, P.H., (2018). End-in-sight: Cell polarization by the polygamic organizer Popz. *Trends Microbiol.*, 26, 363–375.
- Bowman, G.R., Comolli, L.R., Zhu, J., Eckart, M., Koenig, M., Downing, K.H., et al., (2008). A polymeric protein anchors the chromosomal origin/ParB complex at a bacterial cell pole. Cell, 134, 945–955.
- Ebersbach, G., Briegel, A., Jensen, G.J., Jacobs-Wagner, C., (2008). A self-associating protein critical for chromosome attachment, division, and polar organization in caulobacter. Cell. 134, 956–968.
- Bowman, G.R., Perez, A.M., Ptacin, J.L., Ighodaro, E., Folta-Stogniew, E., Comolli, L.R., et al., (2013). Oligomerization and higher-order assembly contribute to sub-cellular localization of a bacterial scaffold. *Mol. Microbiol.* 90, 776–795.
- Lim, H.C., Bernhardt, T.G., (2019). A PopZ-linked apical recruitment assay for studying protein-protein interactions in the bacterial cell envelope. *Mol. Microbiol.*, 112, 1757– 1768.
- Holmes, J.A., Follett, S.E., Wang, H., Meadows, C.P., Varga, K., Bowman, G.R., (2016). Caulobacter PopZ forms an intrinsically disordered hub in organizing bacterial cell poles. Proc. Natl. Acad. Sci., 113, 12490–12495.
- Berge, M., Campagne, S., Mignolet, J., Holden, S., Theraulaz, L., Manley, S., et al., (2016). Modularity and determinants of a (bi-)polarization control system from free-living and obligate intracellular bacteria. *Elife*, 5, 31.
- Perez, A.M., Mann, T.H., Lasker, K., Ahrens, D.G., Eckart, M.R., Shapiro, L., (2017). A Localized complex of two protein oligomers controls the orientation of cell polarity. *Mbio.* 8, 16.
- Wang, H.B., Bowman, G.R., (2019). SpbR overproduction reveals the importance of proteolytic degradation for cell pole development and chromosome segregation in Caulobacter crescentus. *Mol. Microbiol.*, 111, 1700–1714.
- Duerig, A., Abel, S., Folcher, M., Nicollier, M., Schwede, T., Amiot, N., et al., (2009). Second messenger-mediated spatiotemporal control of protein degradation regulates bacterial cell cycle progression. *Genes Dev.*, 23, 93–104.
- Bowman, G.R., Comolli, L.R., Gaietta, G.M., Fero, M., Hong, S.-H., Jones, Y., et al., (2010). Caulobacter PopZ forms a polar subdomain dictating sequential changes in pole composition and function. *Mol. Microbiol.*, 76, 173– 189
- Delaglio, F., Grzesiek, S., Vuister, G.W., Zhu, G., Pfeifer, J., Bax, A., (1995). NMRPipe: A multidimensional spectral processing system based on UNIX pipes. J. Biomol. NMR, 6: 277–293
- Lee, W., Tonelli, M., Markley, J.L., (2015). NMRFAM-SPARKY: enhanced software for biomolecular NMR spectroscopy. *Bioinformatics (Oxford, England)*, 31, 1325–1327.
- Yao, J., Dyson, H.J., Wright, P.E., (1997). Chemical shift dispersion and secondary structure prediction in unfolded and partly folded proteins. FEBS Letters, 419, 285–289.
- Schuberf, M., Labudde, D., Oschkinat, H., Schmieder, P., (2002). A software tool for the prediction of Xaa-Pro peptide bond conformations in proteins based on 13C chemical shift statistics. J. Biomol. NMR, 24, 149–154.
- Wishart, D.S., Sykes, B.D., (1994). The 13C Chemical-Shift Index: A simple method for the identification of

- protein secondary structure using 13C chemical-shift data. *J. Biomol. NMR*, **4**, 171–180.
- Marsh, J.A., Singh, V.K., Jia, Z., Forman-Kay, J.D., (2006). Sensitivity of secondary structure propensities to sequence differences between alpha- and gammasynuclein: Implications for fibrillation. *Protein Sci.*, 15, 2795–2804.
- Lee, W., Stark, J.L., Markley, J.L., (2014). PONDEROSA-C/S: client–server based software package for automated protein 3D structure determination. *J. Biomol. NMR*, 60, 73–75
- Mohana-Borges, R., Goto, N.K., Kroon, G.J.A., Dyson, H. J., Wright, P.E., (2004). Structural characterization of unfolded states of apomyoglobin using residual dipolar couplings. *J. Mol. Biol.*, 340, 1131–1142.
- Bhattacharya, A., Tejero, R., Montelione, G.T., (2007).
   Evaluating protein structures determined by structural genomics consortia. *Proteins: Struct. Funct. Bioinf.*, 66, 778–795
- Das, R.K., Pappu, R.V., (2013). Conformations of intrinsically disordered proteins are influenced by linear sequence distributions of oppositely charged residues. *Proc. Natl. Acad. Sci. U. S. A.*, 110, 13392–13397.
- Martin, E.W., Holehouse, A.S., Grace, C.R., Hughes, A., Pappu, R.V., Mittag, T., (2016). Sequence determinants of the conformational properties of an intrinsically disordered protein prior to and upon multisite phosphorylation. *J. Am. Chem. Soc.*, 138, 15323–15335.
- The PyMOL Molecular Graphics System, Version 1.2r3pre, Schrödinger, LLC.
- McGrath, P.T., Iniesta, A.A., Ryan, K.R., Shapiro, L., McAdams, H.H., (2006). A dynamically localized protease complex and a polar specificity factor control a cell cycle master regulator. Cell, 124, 535–547.
- Joshi, K.K., Berge, M., Radhakrishnan, S.K., Viollier, P.H., Chien, P., (2015). An adaptor hierarchy regulates proteolysis during a bacterial cell cycle. *Cell*, 163, 419– 431.
- Joshi, K.K., Battle, C.M., Chien, P., (2018). Polar localization hub protein PopZ restrains adaptordependent ClpXP proteolysis in Caulobacter crescentus. J. Bacteriol. 200
- Taylor, J.A., Wilbur, J.D., Smith, S.C., Ryan, K.R., (2009). Mutations that alter RcdA surface residues decouple protein localization and CtrA proteolysis in Caulobacter crescentus. J. Mol. Biol., 394, 46–60.
- Williamson, M.P., (2013). Using chemical shift perturbation to characterise ligand binding. *Prog. Nucl. Magn. Reson.* Spectrosc., 73, 1–16.
- 64. Xu, H.B., Ye, H., Osman, N.E., Sadler, K., Won, E.Y., Chi, S.W., et al., (2009). The MDM2-binding region in the transactivation domain of p53 also acts as a Bcl-X-L-binding motif. *Biochemistry*, 48, 12159–12168.
- Kriwacki, R.W., Hengst, L., Tennant, L., Reed, S.I., Wright, P.E., (1996). Structural studies of p21Waf1/Cip1/Sdi1 in the free and Cdk2-bound state: conformational disorder mediates binding diversity. Proc. Natl. Acad. Sci. U. S. A., 93, 11504—11509.
- Ptacin, J.L., Gahlmann, A., Bowman, G.R., Perez, A.M., von Diezmann, A.R.S., Eckart, M.R., et al., (2014). Bacterial scaffold directs pole-specific centromere segregation. Proc. Natl. Acad. Sci. U. S. A., 111, E2046–E2055.

- Blair, J.A., Xu, Q.P., Childers, W.S., Mathews, I.I., Kern, J. W., Eckart, M., et al., (2013). Branched signal wiring of an essential bacterial cell-cycle phosphotransfer protein. Structure, 21, 1590–1601.
- 68. Tsokos, C.G., Perchuk, B.S., Laub, M.T., (2011). A dynamic complex of signaling proteins uses polar localization to regulate cell-fate asymmetry in Caulobacter crescentus. Dev. Cell, 20, 329–341.
- Iniesta, A.A., McGrath, P.T., Reisenauer, A., McAdams, H. H., Shapiro, L., (2006). A phospho-signaling pathway controls the localization and activity of a protease complex critical for bacterial cell cycle progression. *Proc. Natl. Acad. Sci. U. S. A.*, 103, 10935–10940.
- Lasker, K., von Diezmann, L., Zhou, X., Ahrens, D.G., Mann, T.H., Moerner, W.E., et al., (2020). Selective sequestration of signalling proteins in a membraneless organelle reinforces the spatial regulation of asymmetry in Caulobacter crescentus. *Nat. Microbiol.*. 5, 418–429.
- Lori, C., Ozaki, S., Steiner, S., Bohm, R., Abel, S., Dubey, B.N., et al., (2015). Cyclic di-GMP acts as a cell cycle oscillator to drive chromosome replication. *Nature*, 523, 236–239.
- Abel, S., Chien, P., Wassmann, P., Schirmer, T., Kaever, V., Laub, M.T., et al., (2011). Regulatory cohesion of cell cycle and cell differentiation through interlinked phosphorylation and second messenger networks. *Mol. Cell*, 43, 550–560.
- Dahal, L., Shammas, S.L., Clarke, J., (2017). Phosphorylation of the IDP KID modulates affinity for KIX by increasing the lifetime of the complex. *Biophys. J.*, 113, 2706–2712.
- Yadahalli, S., Neira, J.L., Johnson, C.M., Tan, Y.S., Rowling, P.J.E., Chattopadhyay, A., et al., (2019). Kinetic and thermodynamic effects of phosphorylation on p53 binding to MDM2. Sci. Rep., 9, 693.
- Sharma, S., Cermakova, K., De Rijck, J., Demeulemeester, J., Fabry, M., El Ashkar, S., et al., (2018). Affinity switching of the LEDGF/p75 IBD interactome is governed by kinase-dependent phosphorylation. Proc. Natl. Acad. Sci. U. S. A., 115, E7053–E7062.
- Kussie, P.H., Gorina, S., Marechal, V., Elenbaas, B., Moreau, J., Levine, A.J., et al., (1996). Structure of the MDM2 oncoprotein bound to the p53 tumor suppressor transactivation domain. Science, 274, 948–953.
- Follis, A.V., Chipuk, J.E., Fisher, J.C., Yun, M.-K., Grace, C.R., Nourse, A., et al., (2013). PUMA binding induces partial unfolding within BCL-xL to disrupt p53 binding and promote apoptosis. *Nat. Chem. Biol.*, 9, 163–168.
- Day, C.L., Smits, C., Fan, F.C., Lee, E.F., Fairlie, W.D., Hinds, M.G., (2008). Structure of the BH3 domains from the p53-inducible BH3-only proteins Noxa and Puma in complex with McI-1. J. Mol. Biol., 380, 958–971.
- Zor, T., De Guzman, R.N., Dyson, H.J., Wright, P.E., (2004). Solution structure of the KIX domain of CBP bound to the transactivation domain of c-Myb. J. Mol. Biol., 337, 521–534.
- Liu, X., Chen, J., Chen, J., (2019). Residual structure accelerates binding of intrinsically disordered ACTR by promoting efficient folding upon encounter. J. Mol. Biol., 431, 422–432.
- Giri, R., Morrone, A., Toto, A., Brunori, M., Gianni, S., (2013). Structure of the transition state for the binding of c-Myb and KIX highlights an unexpected order for a

- disordered system. Proc. Natl. Acad. Sci. U. S. A., 110, 14942–14947
- Bienkiewicz, E.A., Adkins, J.N., Lumb, K.J., (2002). Functional consequences of preorganized helical structure in the intrinsically disordered cell-cycle inhibitor p27(Kip1). Biochemistry, 41, 752–759.
- Mosyak, L., Zhang, Y., Glasfeld, E., Haney, S., Stahl, M., Seehra, J., et al., (2000). The bacterial cell-division protein ZipA and its interaction with an FtsZ fragment revealed by X-ray crystallography. *EMBO J.*, 19, 3179–3191.
- 84. Hsu, W.-L., Oldfield, C.J., Xue, B., Meng, J., Huang, F., Romero, P., et al., (2013). Exploring the binding diversity of intrinsically disordered proteins involved in one-to-many binding. *Protein Sci.: Publ. Protein Soc.*, 22, 258–273.
- Karlsson, E., Andersson, E., Dogan, J., Gianni, S., Jemth, P., Camilloni, C., (2019). A structurally heterogeneous transition state underlies coupled binding and folding of disordered proteins. *J. Biol. Chem.*, 294, 1230–1239.
- Arai, M., Sugase, K., Dyson, H.J., Wright, P.E., (2015). Conformational propensities of intrinsically disordered proteins influence the mechanism of binding and folding. *Proc. Natl. Acad. Sci. U. S. A.*, 112, 9614–9619.
- 87. Lacy, E.R., Filippov, I., Lewis, W.S., Otieno, S., Xiao, L., Weiss, S., et al., (2004). p27 binds cyclin-CDK complexes through a sequential mechanism involving binding-induced protein folding. *Nat. Struct. Mol. Biol.*, 11, 358–364.
- Laloux, G., Jacobs-Wagner, C., (2013). Spatiotemporal control of PopZ localization through cell cycle-coupled multimerization. J. Cell Biol., 201, 827–841.
- Warfield, L., Tuttle, L.M., Pacheco, D., Klevit, R.E., Hahn, S., (2014). A sequence-specific transcription activator motif and powerful synthetic variants that bind Mediator using a fuzzy protein interface. *Proc. Natl. Acad. Sci. U. S.* A., 111, E3506–E3513.
- Rogers, J.M., Oleinikovas, V., Shammas, S.L., Wong, C.T., De Sancho, D., Baker, C.M., et al., (2014). Interplay between partner and ligand facilitates the folding and binding of an intrinsically disordered protein. *Proc. Natl. Acad. Sci. U. S. A.* 111, 15420–15425.
- Acad. Sci. U. S. A., 111, 15420–15425.
  91. Tuttle, L.M., Pacheco, D., Warfield, L., Luo, J., Ranish, J., Hahn, S., et al., (2018). Gcn4-mediator specificity is mediated by a large and dynamic fuzzy protein-protein complex. Cell Rep., 22, 3251–3264.
- Dogan, J., Mu, X., Engstrom, A., Jemth, P., (2013). The transition state structure for coupled binding and folding of disordered protein domains. Sci. Rep., 3, 6.
- Crabtree, M.D., Borcherds, W., Poosapati, A., Shammas, S.L., Daughdrill, G.W., Clarke, J., (2017). Conserved helixflanking prolines modulate intrinsically disordered protein: Target affinity by altering the lifetime of the bound complex. *Biochemistry*, 56, 2379–2384.
- Shoemaker, B.A., Portman, J.J., Wolynes, P.G., (2000). Speeding molecular recognition by using the folding funnel: the fly-casting mechanism. *Proc. Natl. Acad. Sci.* U. S. A., 97, 8868–8873.
- Harmon, T.S., Holehouse, A.S., Rosen, M.K., Pappu, R.V., (2017). Intrinsically disordered linkers determine the interplay between phase separation and gelation in multivalent proteins. eLife, 6
- Kribelbauer, J.F., Rastogi, C., Bussemaker, H.J., Mann, R. S., (2019). Low-affinity binding sites and the transcription factor specificity paradox in eukaryotes. *Annu. Rev. Cell Dev. Biol.*, 35, 357–379.

- Bahrami, A., Assadi, A.H., Markley, J.L., Eghbalnia, H.R., (2009). Probabilistic interaction network of evidence algorithm and its application to complete labeling of peak lists from protein NMR spectroscopy. *PLoS Comput. Biol.*, 5, e1000307.
- Lee, W., Westler, W.M., Bahrami, A., Eghbalnia, H.R., Markley, J.L., (2009). PINE-SPARKY: graphical interface for evaluating automated probabilistic peak assignments in protein NMR spectroscopy. *Bioinformatics (Oxford, England)*, 25, 2085–2087.
- Shen, Y., Bax, A., (2013). Protein backbone and sidechain torsion angles predicted from NMR chemical shifts using artificial neural networks. J. Biomol. NMR, 56, 227–241.
- Louhivuori, M., Pääkkönen, K., Fredriksson, K., Permi, P., Lounila, J., Annila, A., (2003). On the origin of residual dipolar couplings from denatured proteins. *J. Am. Chem. Soc.*, 125, 15647–15650.
   Schwieters, C.D., Bermejo, G.A., Clore, G.M., (2018).
- 101. Schwieters, C.D., Bermejo, G.A., Clore, G.M., (2018). Xplor-NIH for molecular structure determination from NMR and other data sources. *Protein Sci.*, 27, 26–40.
- 102. Nederveen, A.J., Doreleijers, J.F., Vranken, W., Miller, Z., Spronk, C.A., Nabuurs, S.B., et al., (2005). RECOORD: a recalculated coordinate database of 500+ proteins from the PDB using restraints from the BioMagResBank. *Proteins*, 59, 662–672.